Received: 23 December 2023 | *Revised:* 1 March 2024 | *Accepted:* 6 March 2024
DOI: 10.37917/ijeee.21.2.17 *Vol. 21 | Issue 2 | December 2025*

Iraqi Journal for Electrical and Electronic Engineering
Original Article

Open Access
IJEEE University of Basrah College of Engineering

Investigating the Impact of the Air Void Charges on the Surface Electric Field Distribution of the GIS Spacer

Ahmed D. Awad, Dawood N. Saleh*
Electrical Engineering Department, College of Engineering, University of Mosul, Iraq

Correspondance
*Dawood N. Saleh
Electrical Engineering Department, College of Engineering,
University of Mosul, Iraq
Email: dnsaij@uomosul.edu.iq

Abstract
One of the important components of the gas-insulated switchgear (GIS) system are spacers. These insulators are not free from some manufacturing and operational defects that adversely affect their performance, and among these defects is the presence of air voids inside the solid insulator, which may be exposed to high electric fields that may lead to partial discharges within the voids. These partial discharges may cause the accumulation of charges on the surfaces of these insulators, increase the concentration of the electric field, and cause electric flashover across the interface surfaces between the SF6 gas and the solid insulator. With a 2D axisymmetric model based on finite element analysis (FEA) implemented in COMSOL Multiphysics software, this study investigates the impact of the charges that accumulated on the inner surfaces of the void on the electric field distribution of the spacer's interior and exterior surfaces, as their effect is investigated when they are in different size and locations inside the insulator. This effect is more noticeable when the density of charges on the inner surface of the void increases to 1 ($\mu C/m^2$) and the radius is 2 mm. When the void positioned 1 mm from both the inner and outer surfaces of the spacer, the electric field values are 14.55 and 9.4 MV/m, respectively. The impact site on the spacer surface is narrow within 3 mm and depends on the size of the void. The field enhancement factor may reach 2, and its value is higher on the outer surface than on the inner surface.

Keywords
GIS Spacer, Electric Field Distribution, Air Void, Partial Discharge, Surface Flashover.

I. Introduction

Gas-insulated switchgear (GIS) is a crucial element in modern electricity grids as it enables efficient and secure transmission and distribution of electrical energy. GIS comprises SF6-filled equipment, which is widely employed in power transmission networks due to its exceptional reliability and compactness. The insulating spacers present in the GIS are essential components that ensure the equipment's safe and reliable operation [1]. The electric field distribution on the insulating spacer's surface is a critical factor that determines the GIS's insulation performance. Any defects or charge accumulation on the spacer's surface can lead to local electric field enhancement and potential partial discharge (PD) activity, which can cause the failure of the entire GIS [2]. Several factors contribute to the irregular distribution of the electric field on the spacer surfaces within the system. These factors can stem from the insulator or other parts of the system. However, the primary reasons for irregular electric field distribution are internal defects within the spacer that occur during manufacturing or installation processes or while in operation. One notable drawback is that there are voids inside the spacer. These voids can distort the electric field at the spacer surface during partial discharge states. This occurrence stems from the electric field concentration within these voids due to differences in the dielectric constant [3]. Numerous investigations have examined the relationship between the distribution of the electric field inside the void and the accumulation of charges on its inner surface as a result of partial discharges [4–7].

In a solid dielectric, Elias et al. [8, 9] investigated the partial discharge (PD) behavior inside a spherical cavity. The study examines the mechanisms underlying intra-cavity PD and how it responds to changes in the applied voltage's frequency and amplitude. The findings demonstrate that it is possible to determine both theoretically and practically the number of PDs per cycle, the overall magnitude of charges per cycle, and the maximum charge magnitude. The study of Nguyen and Phuong [10] investigated the comparison of internal discharge in a cylindrical void surrounded by a solid dielectric material based on cavity size and applied voltage at 50 Hz and VLF. The applied frequency and voltage rise rate are found to have a significant influence on the PD behaviors. PD magnitudes, independent of voltage waveforms, are typically smaller at very low frequencies (VLF) than at power frequency. They suggest that the larger cavity may increase the number of low-level discharges by increasing the surface area of the discharge. The geometrical void structure affects discharge characteristics like inception level, magnitude, and repetition rate. Sharp corners in voids intensify stress points, affecting free electron availability and initiating more PDs. Partial discharge inception voltage (PDIV) values depend on cavity geometry and excitation frequency, with higher cavity surfaces exhibiting larger PD magnitudes. Therefore, cavity geometry, associated cavity surface area, charge concentration locations, and increased electric stress all have a significant impact on PD properties [11]. Umemoto et al. examined the connection between void volume and insulation lifetime. Insulation longevity testing was done on samples with different internal void sizes as part of the investigation. The authors also computed the n-value indices and insulating lifespan of the V-t characteristics for a range of void volumes. The study also assessed the correlation between the energy of partial discharge (PD) features occurring in the void and the insulating lifetime. The results of the insulating lifespan characteristics indicated a decrease in the n-value index of V-t characteristics as the void volume increased. Furthermore, the results demonstrated a direct correlation between the cumulative PD power density per cycle of the applied voltage and the insulation lifespan of insulators with voids [12]. On the other hand, many theoretical and practical studies have been conducted to explore the effects that lead to irregular electric field distribution on the spacer surfaces [13–17]. Li et al. [18] explore surface charge accumulation and its impact on surface flashover in compressed gases, summarizing literature, examining factors affecting accumulation and measurements, and analyzing surface charge effects on surface breakdown under different voltage waveforms. They come to the conclusion that it is yet unknown what aspect of the surface charge distribution is most damaging to surface flashover. In other words, it's important to comprehend the impact of the presence of surface charges with various polarities in various concentrations on the phenomenon of surface discharge. In order to prevent charge accumulation in gas insulated transmission lines (GIL), Zuodong Liang et al. [19] suggest a design approach for a DC spacer. Simulated and type testing demonstrate reduced surface electric flux and surface charge in comparison to AC spacers, and a prototype is produced and evaluated. The test findings confirm that this DC spacer has a larger surface flashover voltage than the AC spacer. The design's potential viability for HVDC gas-insulated equipment is discussed in the study. Afrouzi et al. [20] provide an overview of partial discharge dynamics (PD) and discuss various modeling techniques. The foundational concepts are based on Niemeyer's model, and PRPD patterns are generated through experiments. However, some models have limitations and inconsistencies. The Poisson PD model, resolved using FEA, is chosen over Niemeyer's, ABC, Pedersen, and Plasma models due to its ability to resolve defect geometry. Finding finite element method (FEM) models suitable due to cost and low application, but FEM's accuracy requires large data during meshing. The study in GIS/GIL revealed that the insulation breakdown of epoxy-based spacers is closely linked to electric field distortion under various voltage waveforms and temperature gradients. The basin-type spacer's surface charge polarity is influenced by gas transmission, with the upper surface experiencing opposite polarity due to increasing spacer conductivity with temperature, causing a density drop or polarity reversal. The electric field distribution distortion at the triple junction in epoxy spacers is exacerbated by temperature-dependent volume conductivity, necessitating the use of shielding electrodes for field grading [21]. These investigations mainly focused on the individual effects of surface charges or void charges, but the combined effect was not significantly paid attention to. The main aim of the present work is focusing on how the partial discharges within voids close to the inner or outer surfaces of a spacer in a GIS can drastically alter the distribution of the electric field at the spacer surface. The influence of cavity charges on the surface electric field distribution of the GIS spacer was investigated in this study using theoretical simulation techniques. In order to solve a two-dimensional axisymmetric model, one such technique is finite element analysis (FEA), which entails modeling the GIS spacer and surrounding electric field by applying mathematical equations and numerical techniques using the COMSOL Multiphysics software [22]. Investigating the effect of cavity charges on the surface electric field distribution of a GIS spacer has significant practical implications for the safe and reliable operation of the equipment. By understanding the mechanisms and effects of cavitation charges, researchers can develop new diagnostic techniques and isolation materials to prevent PD from occurring and reduce the risk of GIS failure.

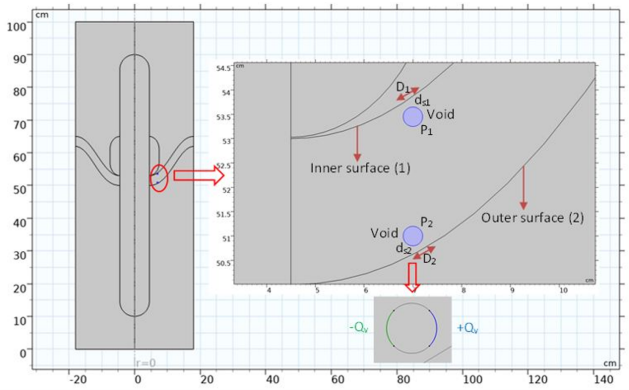

Fig. 1. The fundamental 2-D axisymmetric computational model of a GIS

II. Model Description

A. Model Geometry

The basic 2-D computational model of a GIS is shown in Fig. 1. An epoxy-alumina composite GIS spacer, a GIS shell, a center conductor, a shielding ball, and SF6 gas are all included in the model of a GIS component. The center conductor is 900 mm long, while the GIS segment is 1000 mm long. The relative permittivity of the epoxy-alumina composite and SF_6 are 5.9 (50 Hz, 25 °C) and 1.002, respectively. The spacer normally has a basin form and measures 130 mm in axial length and 30 mm in thickness. The internal diameter of the shell is 360 mm, while the exterior diameter of the center conductor is 90 mm. To simplify the modeling and calculation workload, certain bolt connections between the metal parts were excluded, as they have a negligible impact on the electric field distribution [23].

B. Void Geometry and Location

The locations of the spacer's voids are shown in Fig. 1, and the impact of each void was evaluated independently between the inner (concave) and outer (convex) surfaces of the spacer at a distance of between 1 and 6 mm from the surface. The concave inner surface of the spacer was given the number 1, while its convex outer surface was given the number 2. The normal and tangential electric fields are denoted by the letters (n) and (t), respectively. P_1 is close to the inner surface, while void P_2 is close to the exterior surface. The centers of the voids were altered in accordance with their radii while maintaining a fixed distance between their perimeters and either their inner or outer surfaces. The voids were created as spheres with 1- and 2-mm radii. Air fills these areas when the atmospheric pressure is normal.

C. Initial and Boundary Conditions

Accurately measuring electric charges within a cavity contained within an insulator is a challenging task. The partial discharge that occurs inside the cavity can have a great effect on the charge distribution. Accurately calculating the amount of charges produced inside the cavity requires conducting complex practical experiments or lengthy simulations that require a lot of effort and time in order to analyze the results of the plasma resulting from partial discharges by knowing the particles contributing to the conduction process and their rate of production of negative and positive ions. Therefore, it is necessary to adopt certain values taken from previous reliable studies and considered constants in simulating and analyzing the resulting data. This simplifies the analysis process and helps predict the behavior of the system under different conditions. However, this approach may increase the level of approximation in the results and is considered a challenge for the electrical equipment industry, which relies heavily on accurate measurements of electrical charges in insulation systems. Since the range of these charges runs from 1700 to 4000 pC every cycle [8], the quantity of charges that build up on the inner surfaces of the void directly depends on the frequency and degree of partial discharges. With these numbers, the surface charge density of the void was calculated and set to Q_v = 0, 300, 500, 700, and 1000 (μC/m^2). These values have been calculated based on the minimum and maximum values of the charges resulting from partial discharges that occur during one cycle of the applied voltage, which range from 1700 to 4000 pC [8] . Thus, most degrees of partial discharges that occur within the void, from light to severe discharges, are covered, including the case when no partial discharge occurs. These charges are positioned perpendicular to the electric field lines, with -Q_v on the portion of the gap surface nearest to the central conductor and +Q_v on the outside quadrant. The primary conductor of the system is supplied with a 400 kV voltage, and the exterior wall is connected to earth.

III. Electrical Field Calculation

A gas-insulated system's electric field can be described using the Poisson's equation, which links the electric field to the system's charge density [1]:

$$\nabla.(\varepsilon \nabla V) = -\rho \tag{1}$$

where ε is the permittivity of the gas, ρ is the charge density, and V is the electric potential. Knowing the electric potential allows one to determine the electric field using the gradient of the electric potential, which is given by [1]:

$$E = -\nabla V \tag{2}$$

The electric field distribution of a gas-insulated system can be described by Gauss's law, which relates the electric field to

the charge density according to the following equation [1]:

$$\nabla.E = \frac{\rho}{\varepsilon} \tag{3}$$

The degree of polarization of the system's dielectric materials in the presence of an applied electric field demonstrates the significance of these materials' relative permittivity and the extent to which it affects how the electric field is distributed within the system. Charges within the dielectric material (epoxy) undergo a displacement when an external electric field (E_{app}) is supplied to the system. This displacement of charges creates an internal electric field (E_{pol}) that opposes the applied field. The net electric field within the material, known as the total electric field (E_{tot}), is the vector sum of the applied and internal electric fields [24, 25]:

$$E_{tot} = E_{app} + E_{pol} \tag{4}$$

The relationship between polarization (P), electric susceptibility (χ), and the applied electric field (E_{app}) can be expressed using the equation [24]:

$$P = \varepsilon.\chi.E_{app} \tag{5}$$

Where the electric susceptibility (χ) is related to the dielectric constant (ε_r) or relative permittivity of the material through the formula [24]:

$$\varepsilon_r = 1 + \chi \tag{6}$$

Polarization modifies the total electric field distribution within the dielectric material. The internal electric field due to polarization opposes the applied field, leading to reduced effective field strengths within the material. This effect becomes significant when analyzing the behavior of the electric field within the spacer-air void system.

Since the system has a cylindrical shape, it is mathematically subject to the cylindrical axes in calculating the electric field resulting from applying a voltage (V_{app}) to the central conductor of the system. Therefore, the applied electric field (E_{app}) can be calculated as follows [24]:

$$E_{app} = \frac{V_{app}}{r \ln\left(\frac{r_2}{r_1}\right)} \tag{7}$$

Where r_1 and r_2 are the radius of the central conductor and the outer wall respectively. In the absence of charges inside the void, the distribution of the electric field depends on the differences in the relative permittivity of the air inside the void and the epoxy material and can be calculated as follows [3]:

$$E_v = \frac{3E_{app}\ \varepsilon_e}{(\varepsilon_v + 2\ \varepsilon_e)} \tag{8}$$

Where the ε_v and ε_e are the permittivity of the void (air) and the epoxy spacer respectively. As for the presence of charges inside the void resulting from partial discharges, the distribution of the electric field depends on the nature of the charges and how they are accumulated on the inner surfaces of the void. The idea of symmetry can be taken into consideration in this particular circumstance to make the calculation simpler. It is possible to use symmetry to simplify the computations since the distribution of charges on the inner surface of the void has a setup with quarter-circumference positive and negative charges. The vector sum of the applied electric field, the electric fields created by the positive charges, and the electric fields created by the negative charges will equal the electric field that is present on the surface of the spacer. On the surface of the spacer, the contributions from each field component will produce both normal and tangential fields. Coulomb's law can be used to determine the electric field at any point on the spacer surface caused by a small charge element dq along a quarter of the circle [3]:

$$d\hat{E} = \frac{1}{4\pi\varepsilon_o}\frac{dq}{r^2}\hat{r} \tag{9}$$

Where:
- $d\hat{E}$is the infinitesimal electric field vector due to the charge element.
- dq is the infinitesimal charge element.
- r is the distance from the charge element to the point on the spacer's surface where you're calculating the field.
- $\hat{r}$ is the unit vector pointing from the charge element to the point on the spacer's surface.

The overall electric field at a given position on the surface of the spacer can be calculated by integrating the contributions from each charge element along the quarter-circumference. The vector components of the electric fields produced by each charge element are added to produce the overall electric field that can be seen on the surface of the spacer. However, the problem becomes quite complex due to the non-uniform distribution of charges and the trigonometric relationships involved. Calculating the electric field analytically along a portion of the spacer surface would require detailed integration and trigonometric manipulation. For accurate results, utilizing simulation software can accurately calculate the electric field distribution in this system. Therefore, modeling of the system is done by using the COMSOL Multiphysics program to solve a 2D axisymmetric model.

IV. Results and Discussion

This study investigated the distribution of electric field on the surface of spacers in several cases, including the absence of any air void within the insulating material of the spacer

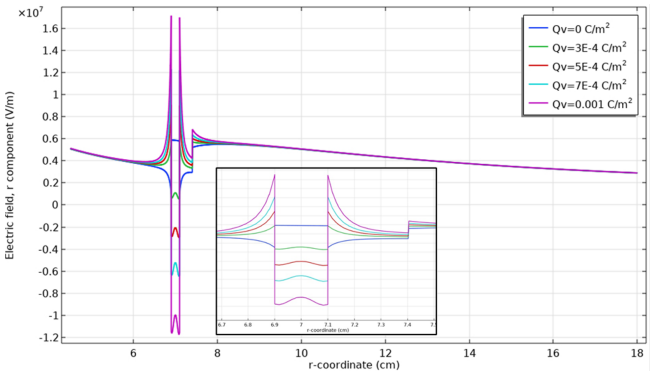

Fig. 2. Air void electric field with different charge density.

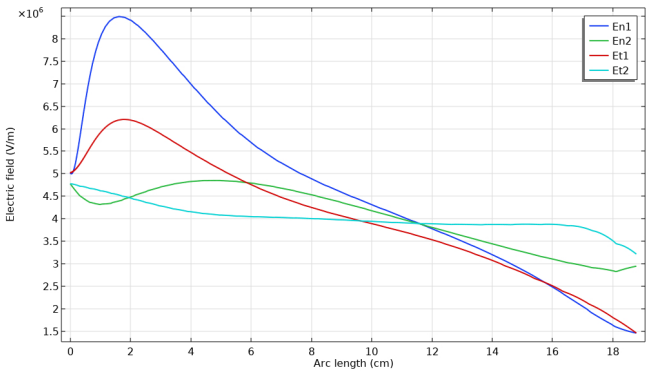

Fig. 3. Electric field distribution on the inner and outer surfaces of the spacer with no air void.

as well as the presence of one air void at two locations, as indicated in Fig. 1. The density of charges accumulated on the inner surface of the void changes from zero charge in the case of no partial discharge occurring within the void to 1000 μC/m^2, depending on the severity of the partial discharge inside the void. The effect of void size on the distribution of the electric field was also studied, assuming fixed values of charge density. The effect of increasing the separation distance between the void and the spacer surfaces (d$s_{1,2}$) on the electric field distribution on the spacer surface has been studied.

A. Electric Field Inside Air Void

Depending on whether there are space charges present inside the void or not, the electric field of the air void can be distinguished. Due to the polarization processes of the spacer materials, which result in varying permittivity, the value of the electric field inside the vacuum is greater than that in the surrounding solid dielectric. The polarity of the applied voltages and the charges, however, have an impact on the electric field when a partial discharge takes place inside the void and charges build up on its inner surface, as depicted in Fig. 2. Particularly when the void is relatively close to the spacer surfaces, the electric field inside the void can have an impact on the field distribution over those surfaces.

Fig. 2 represents the electric field along the radial line between the central conductor and the grounded wall, passing through the center of the void. Although the boundary conditions differ between the models, it is possible to compare some results that are subject to scaling operations, such as the field enhancement factor, whose value inside the spherical air void as shown in Fig. 2 is in the range of 1.5. This value is close to the value obtained from references [26, 27] where the enhancement factor of the void was in the range of around 1.32.

B. Spacer Without Air Void

In the case of absence of any air void inside the spacer, the electric field distribution on a spacer's interior and exterior surfaces is shown in Fig. 3. Whether the field is normal or tangential, it is obvious that the electric field on the inner surface is greater than that on the outer surface. The paths that the electric field lines traveling from the system's central conductor take are what cause the inner surface to be closer and the field to be stronger. Both surfaces had a stronger electric field that was concentrated near the busbar, or the central conductor, and dwindled as it traveled outward toward the outer wall. The type of boundary conditions the electric field lines encounter at the surfaces of the spacer should also be considered. At the inner surface, a gaseous insulator changes to a solid insulator, while at the outer surface, a solid insulator changes to a gaseous insulator. Because of this, the two insulators' different relative permittivity values result in different electric field values on the spacer's two surfaces. The findings in this case follow a similar trend to those found in reference [28].

C. Air Void Near the Spacer Outer Surface (P_2)

Fig. 4 and Fig. 5 show, respectively, the normal and tangential electric fields on a spacer's outer surface, under the influence of an air void with a radius of r_v=1 mm at position P_2, d_{s2}=1 mm away from the edge as shown in Fig. 1. The surface charge density on the inner surface of the void is indicated in the figures. It is clear that the electric field on the surface of the void changes significantly within a short distance on the surface, where this change is proportional to the number of charges accumulated on the inner surface of the void, the more charges on the inner surface of the void, the higher the value of the electric field on the surface of the spacer. The behavior of the field is similar in all cases, where the field decreases to a minimum value and then starts to increase. This is due to the polarity difference of the charges on the

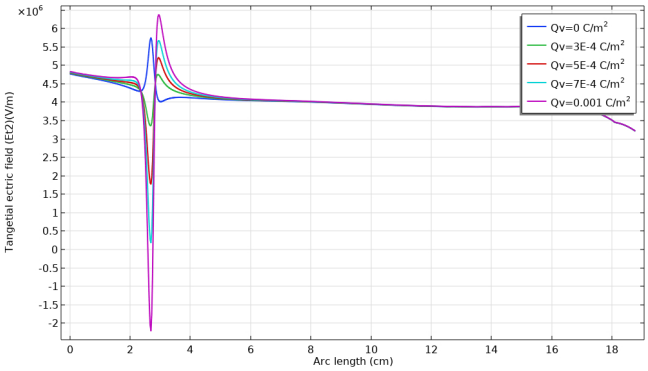

Fig. 4. The normal electric field on the outer surface of the spacer.

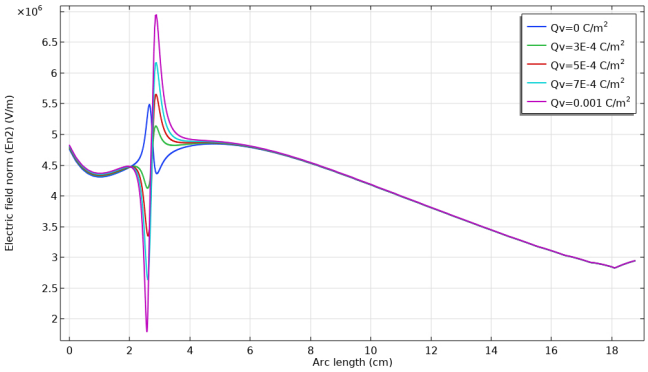

Fig. 5. The tangential electric field on the outer surface of the spacer.

surface of the void, which generates electric fields opposite and mutually supportive with the main field resulting from the central conductor. In the case of the absence of charges inside the void, the behavior of the electric field on the surface of the spacer is different from the previous cases, where it first increases and then decreases until it stabilizes at the final value. The change in the value of the field in this case depends on the dielectric constant of the void and the spacer.

As mentioned previously, the effect appears within a narrow range on the surface of the spacer, and this range is represented by the distance ($D_{n,t2}$) between the two points at which the maximum and minimum value of the electric field occurs, as shown in Table I and Table II. For tangential field the D_{t2} is equal 2.6mm while for normal component the D_{n2} has values changed from 2.5mm to 3.2mm. The amount of distortion in the electric field appears clear from the values of the field enhancement factor, as it increases with the increase in the density of the charges of the void.

$$f = \frac{E_{n,tmax}}{E_{n,tav}} \tag{10}$$

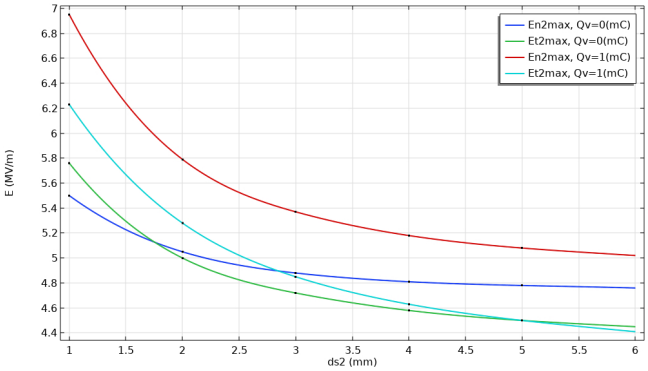

Fig. 6. Normal and tangential electric field for different spacing between void and the outer spacer surface.

- where f is the field enhancement factor.
- $E_{n,tmax}$ is the maximum normal and tangential field.
- $E_{n,tav}$ is the average normal and tangential field with spacer free of void.

Both the normal and tangential fields have field enhancement factor value approach to 1.5 which makes the spacer surface susceptible to flashover that may lead faulty system. The effect of the position of the void from the outer surface of the spacer is shown in the Table III and Fig. 6, where a rapid decrease in field values is observed with increasing separation distance, especially between d_s = 1mm and d_s = 3mm, while the decrease after d_s = 3mm is slower. The field settle towards the values shown in Fig. 3 after the maximum and minimum values resulting from the effect of the void vanished. This result is consistent with the equation of a number where the field is proportional to the inverse square of the distance between the charges, which are the source of the field, and the site of influence on the surface of the spacer.

It also seems clear that the presence of charges on the surface of the gap is more effective when the gap is closer to the surface of the spacer. The worst case in terms of the high

TABLE I.
MAXIMUM AND MINIMUM TANGENTIAL FIELD ON THE OUTER SURFACE WHEN $r_v = 1mm$, $d_{s2} = 1mm$, $E_{tav} = 4.32(MV/m)$

Q_v (μC/m^2)	E_{t2max} (MV/m)	E_{t2min} (MV/m)	D_{t2} (mm)	f= E_{t2max}/E_{t2av}
0	5.75	4	2.6	1.33
300	4.75	3.36	2.6	1.10
500	5.21	1.77	2.6	1.21
700	5.68	0.18	2.6	1.31
1000	6.38	-2.22	2.6	1.48

TABLE II.
MAXIMUM AND MINIMUM NORMAL FIELD ON THE OUTER SURFACE WHEN $r_v = 1mm$, $d_{s2} = 1mm$, $E_{tav} = 4.65(MV/m)$

Q_v ($\mu C/m^2$)	E_{n2max} (MV/m)	E_{n2min} (MV/m)	D_{n2} (mm)	f= E_{n2max}/E_{n2av}
0	5.5	4.36	2.5	1.18
300	5.14	4.13	3	1.11
500	5.65	3.35	3	1.22
700	6.17	2.64	3	1.33
1000	6.94	1.79	3.2	1.49

TABLE III.
NORMAL AND TANGENTIAL ELECTRIC FIELD FOR DIFFERENT SPACING BETWEEN VOID AND THE OUTER SPACER SURFACE

d_{s2} (mm)	Q_v=0 ($\mu C/m^2$)		Q_v=1000 ($\mu C/m^2$)	
	E_{n2max} (MV/m)	E_{t2max} (MV/m)	E_{n2max} (MV/m)	E_{t2max} (MV/m)
1	5.5	5.76	6.95	6.23
2	5.05	5	5.79	5.28
3	4.88	4.72	5.37	4.85
4	4.81	4.58	5.18	4.63
5	4.78	4.5	5.08	4.5
6	4.76	4.45	5.02	4.41

value of the electric field on the surface of the spacer occurs when the void is as close as possible to the surface of the spacer, where the distance between the circumference of the void and the surface of the spacer is within 1 mm. Therefore, the effect of the size of the void will be studied at this location, i.e., keeping the distance Within 1 mm with a change in the radius of the void to r_v=2mm and maintaining the same values of the charge density on the inner surface of the gap. The normal electric field distribution is shown in Fig. 7, the effect of the size of the void on the distribution of the electric field on the surface of the spacer can be seen inside the square dotted ellipse, where the effect of size appears clearly in the Fig. 7b and covers a larger area of the surface of the spacer with larger field values equal 9.4 MV/m.

To show the amount of change in the electric field on the surface of the spacer, whether the field is normal or tangential, with the change in the values of the charges on the inner surface of the largest gap, we can refer to the Fig. 8 and Fig. 9, respectively.

From the figures, it can be seen that the normal field and

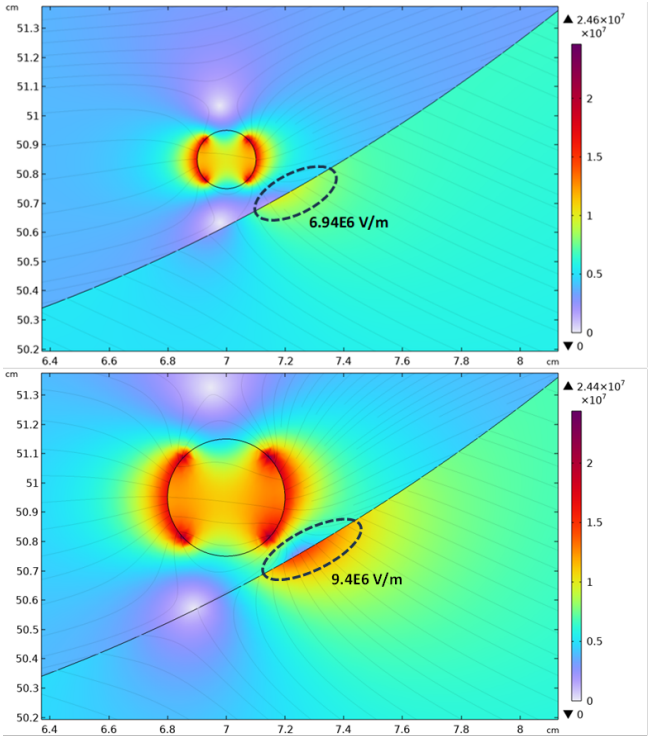

Fig. 7. Normal electric field on the outer surface for (a) r_v=1mm and d_{s2}=1mm, (b) r_v=2mm and d_{s2}=1mm.

the tangential have the same behavior as the previous case r_v=1mm, but with higher values in the case of increase and lower values in the case of decrease, with a larger area of influence on the surface of the spacer, as the values of $D_{n,t}$ are larger, as shown in Table IV and Table V. The amount of increase in the electric field on the surface of the spacer, resulting from the increase in the size of the void, can be seen through the values of the field enhancement factor, which are fixed in Table IV and Table V, as its value exceeds 2 in the case of the highest value of the charge density, which was within the limits of 1.5 in the previous case, as the increase is not proportional to the increase in the size of the void.

D. Air Void Near the Spacer Inner Surface (P_1)

In the case of presence an air gap near the inner surface of the spacer leads to the opposite effect of what happens in the case of its presence near the outer surface. Whereas, the value of the field on the surface of the spacer increases at the beginning to the highest value, then begins to decrease to the lowest value, and then returns to settle at the final value of the field for each of the normal and tangential fields, as shown in the Fig. 10 and Fig. 11. The increase in the field at the beginning was the result of the vector sum of the main field resulting from the central conductor and the field resulting from the

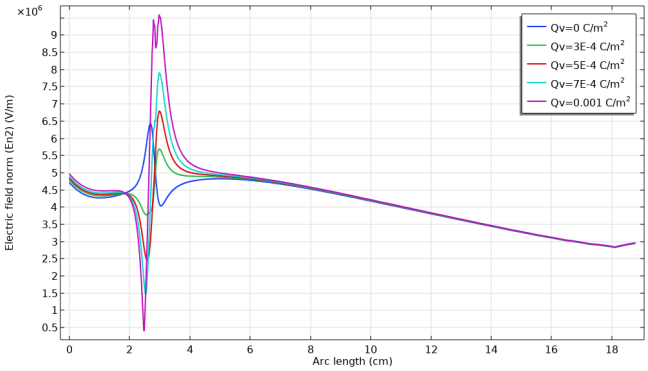

Fig. 8. Normal electric field along the outer surface of the spacer with r_v=2mm and d_{s2}=1mm.

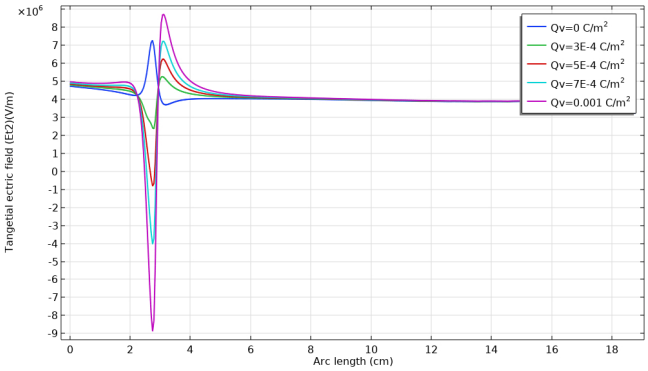

Fig. 9. Tangential electric field along the outer surface of the spacer with $r_v = 2mm$ and $d_{s2} = 1mm$.

negative charges that are close to the central conductor, and in both cases the field lines enter the inner surface of the spacer. As for the field lines resulting from the positive charges, they are emerging from the surface of the spacer, which leads to a decrease in the resultant electric field on the surface of the spacer. Therefore, the field increases on the surface close to the negative charges of the void and decreases on the surface near the positive charges of the void, and this is completely opposite to what happens on the outer surface.

The amount of distortion in the electric field increases with the increase in the density of charges on the inner surface of the void, but it remains the same behavior for all values of charge densities, as shown in the Fig. 10 and Fig. 11. The values of the field enhancement factor, which are found in the Table VI and Table VII, reflect the amount of change in the field on the inner surface of the spacer, where it reaches its maximum value 1.45 for the tangential field and 1.38 for the perpendicular field, and these values remain less than the values obtained in the case of the outer surface and all this for distance between the void and inner surface of the spacer equal d_{s1}=1mm. Increasing the size of the void by increasing

TABLE IV.
MAXIMUM AND MINIMUM TANGENTIAL FIELD ON THE OUTER SURFACE WHEN $r_v = 2mm$, $d_{s2} = 1mm$, $E_{tav} = 4.32(MV/m)$

Q_v ($\mu C/m^2$)	E_{t2max} (MV/m)	E_{t2min} (MV/m)	D_{t2} (mm)	f= E_{t2max}/E_{t2av}
0	7.26	3.69	3.5	1.68
300	5.25	2.35	3.5	1.22
500	6.24	-0.8	3.5	1.44
700	7.23	-4	3.5	1.67
1000	8.7	-8.86	3.5	2.01

TABLE V.
MAXIMUM AND MINIMUM TANGENTIAL FIELD ON THE OUTER SURFACE WHEN $r_v = 2mm$, $d_{s2} = 1mm$, $E_{tav} = 4.65(MV/m)$

Q_v ($\mu C/m^2$)	E_{n2max} (MV/m)	E_{n2min} (MV/m)	D_{n2} (mm)	f= E_{n2max}/E_{n2av}
0	6.45	4.04	3.5	1.39
300	5.7	3.77	3.5	1.23
500	6.8	2.45	3.5	1.46
700	7.92	1.47	4	1.70
1000	9.4	0.42	4.5	2.06

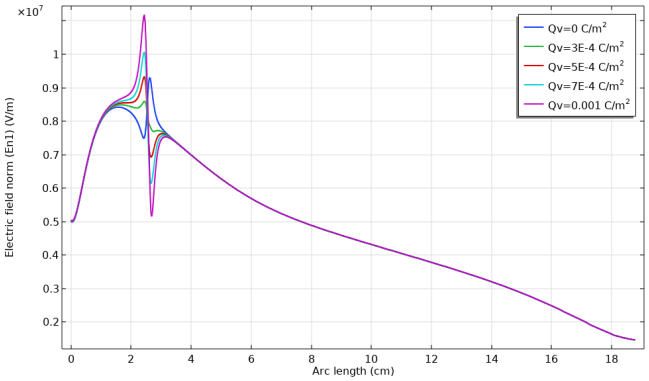

Fig. 10. Normal electric field along the inner surface of the spacer with $r_v = 1mm$ and $d_{s1} = 1mm$

its radius to r_v=2 mm while maintaining the same density of charges on its inner surface directly affects the distribution of the electric field on the inner surface of the spacer, and this effect is greater than the previous case, i.e. the radius of the void is r_v=1 mm, and this is shown in the Fig. 12 and Fig. 13 for normal and tangential field respectively. The maximum normal field values may reach 14.55 MV/m, while the maximum tangential field values may reach 11.73 MV/m

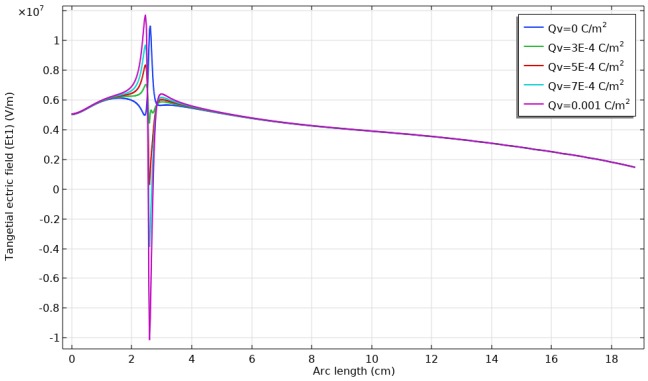

Fig. 11. Tangential electric field along the inner surface of the spacer with $r_v = 1mm$ and $d_{s1} = 1mm$

when the charge density is equal to Q_v=1000 μC/m^2.

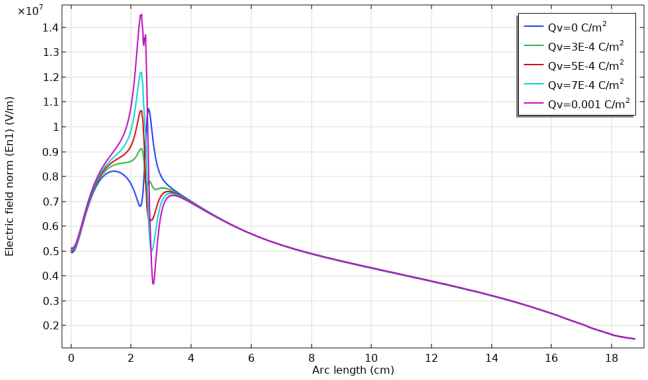

Fig. 12. Normal electric field along the inner surface of the spacer with $r_v = 2mm$ and $d_{s1} = 1mm$.

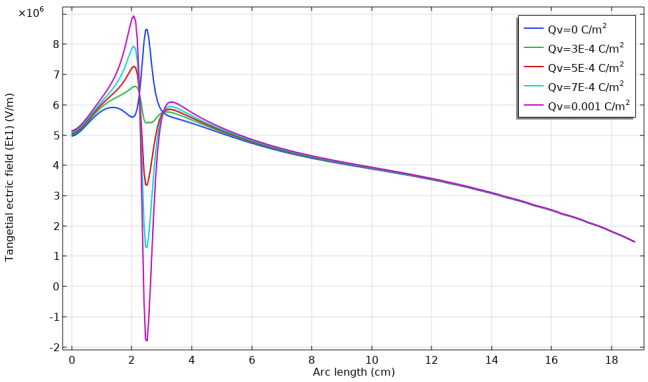

Fig. 13. Tangential electric field along the inner surface of the spacer with $r_v = 2mm$ and $d_{s1} = 1mm$.

The increase in the electric field magnitude on the inner surface of the spacer resulting from the increase in the size of the void can be inferred from the values of the field enhancement factor which are fixed in the Table VIII and Table IX and these values are greater than the values of the previous case when the void was smaller. Although the maximum values of the field, whether the field is normal or tangential on the inner surface of the spacer, are greater than the maximum values that appear on the outer surface of the spacer, the values of the field enhancement factor are less in the case of the inner surface of the spacer than the outer surface, and this is shown in the Fig. 14.

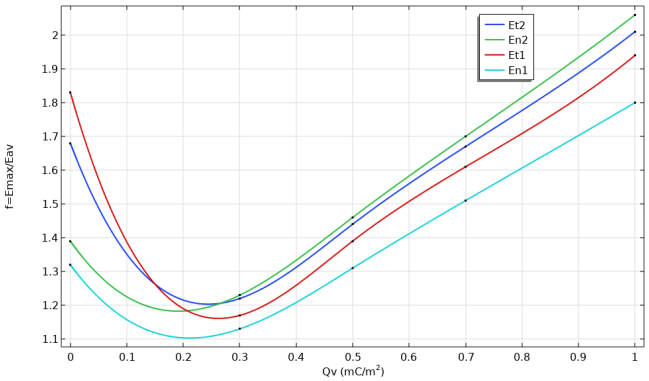

Fig. 14. The field enhancement factor for both normal and tangential field on the inner and outer surfaces, $r_v = 2mm$ and $d_s = 1mm$.

The field enhancement factor increases linearly with the increase in the density of charges on the inner surfaces of the void, but in the absence of charges inside the void, this factor is greater in the case of the tangential field than the normal field for the two surfaces of the spacer. The reason behind this is the charges that appear at the edge of the void as a result of the polarization of the dielectric materials of the spacer when exposed to the main applied field from the central conductor of the system.

Fig. 15 illustrates the typical distribution of the normal electric field. The impact of void size on this distribution

TABLE VI.
MAXIMUM AND MINIMUM TANGENTIAL FIELD ON THE INNER SURFACE WHEN $r_v = 1mm$, $d_{s1} = 1mm$, $E_{tav} = 6.05(MV/m)$

Q_v (μC/m^2)	E_{t2max} (MV/m)	E_{t2min} (MV/m)	D_{t2} (mm)	f= E_{t2max}/E_{t2av}
0	8.5	5.54	2	1.40
300	6.58	5.41	2	1.09
500	7.23	3.35	2	1.20
700	7.9	1.28	2	1.31
1000	8.8	-1.81	2	1.45

TABLE VII.
MAXIMUM AND MINIMUM NORMAL FIELD ON THE INNER SURFACE WHEN $r_v = 1mm$, $d_{s1} = 1mm$, $E_{tav} = 8.1(MV/m)$

Q_v ($\mu C/m^2$)	E_{n2max} (MV/m)	E_{n2min} (MV/m)	D_{n2} (mm)	f= E_{n2max}/E_{n2av}
0	9.3	7.5	2.2	1.15
300	8.6	7.69	3	1.06
500	9.33	6.92	2.5	1.15
700	10.05	6.14	2.5	1.24
1000	11.17	5.16	2.5	1.38

across the spacer's surface is highlighted within the square-dotted ellipse. Notably, the influence of void size is particularly evident in Fig. 15b, encompassing a broader region of the spacer's surface. This area exhibits higher field values, reaching up to 14.55 MV/m.

TABLE VIII.
MAXIMUM AND MINIMUM TANGENTIAL FIELD ON THE INNER SURFACE WHEN $r_v = 2mm$, $d_{s1} = 1mm$ AND $E_{t1av} = 6.05(MV/m)$

Q_v ($\mu C/m^2$)	E_{t2max} (MV/m)	E_{t2min} (MV/m)	D_{t2} (mm)	f= E_{t2max}/E_{t2av}
0	11.1	4.96	3.3	1.83
300	7.05	4.26	2.3	1.17
500	8.39	0.29	2.3	1.39
700	9.73	-3.8	2.3	1.61
1000	11.73	-10.12	2.3	1.94

The increase in the separation distance between the void and the inner surface of the spacer is shown in Table X and Fig. 16, as the field values decrease rapidly when the distance is less than 3 mm, while the decrease is slower after that. A comparison was made for two cases, which is in the case of the presence of the largest amount of charges inside the void and in the absence of any charge. It appears from the Fig. 16 that the normal field on the inner surface of the spacer, in the case of the presence of charges, is the highest in value, followed by the normal field in the absence of charges. The effect of the spacing between the void and the inner surface on the tangential field is almost identical for the two cases, i.e. in the presence and absence of charges.

V. CONCLUSIONS

For the purpose of simulating the impact of a sphere-shaped air gap inside an epoxy GIS spacer, a two-dimensional axisymmetric model has been developed. The existence of charges on the inner surface of the void has an impact on the distribution of the electric field on the spacer's surface. The amount of charges that have accumulated on the inner surface of the void are directly correlated with how the electric field behaves over a short distance on the spacer's surface. The variation of the electric field is measured by the field enhancement factor (f). This component is increased by the presence of charges on the void's surface, with larger charge densities resulting in greater field enhancement.

The spacer's surface is prone to flashover, which could result in system faults, as both the normal and tangential electric fields have enhancement factors that are close to 1.5. The influence of the void's distance from the spacer's surface is investigated, and it is found that field values rapidly decline with growing separation distance, following an inverse square relationship similar to the equation regulating the interaction of charges. The effect of the void's size on the distribution of the electric field is also examined in this study. The field enhancement factor can be greater than 2 in situations with

TABLE IX.
MAXIMUM AND MINIMUM NORMAL FIELD ON THE INNER SURFACE WHEN $r_v = 2mm$, $d_{s1} = 1mm$ AND $E_{n1av} = 8.1(MV/m)$

Q_v ($\mu C/m^2$)	E_{n2max} (MV/m)	E_{n2min} (MV/m)	D_{n2} (mm)	f= E_{n2max}/E_{n2av}
0	10.73	6.79	3	1.32
300	9.13	7.48	3	1.13
500	10.65	6.23	3	1.31
700	12.22	5.02	3.5	1.51
1000	14.55	3.67	4	1.80

TABLE X.
NORMAL AND TANGENTIAL ELECTRIC FIELD FOR DIFFERENT SPACING BETWEEN VOID AND THE INNER SPACER SURFACE

ds1 (mm)	Q_v=0 ($\mu C/m^2$)		Q_v=1 ($\mu C/m^2$)	
	E_{n1max}, (MV/m)	E_{t1max} (MV/m)	E_{n1max} (MV/m)	E_{t1max} (MV/m)
1	9.3	8.5	11.17	8.8
2	8.61	7.14	9.61	7.38
3	8.39	6.68	9.11	6.86
4	8.32	6.47	8.91	6.36
5	8.3	6.36	8.82	6.05
6	8.29	6.31	8.76	6.41

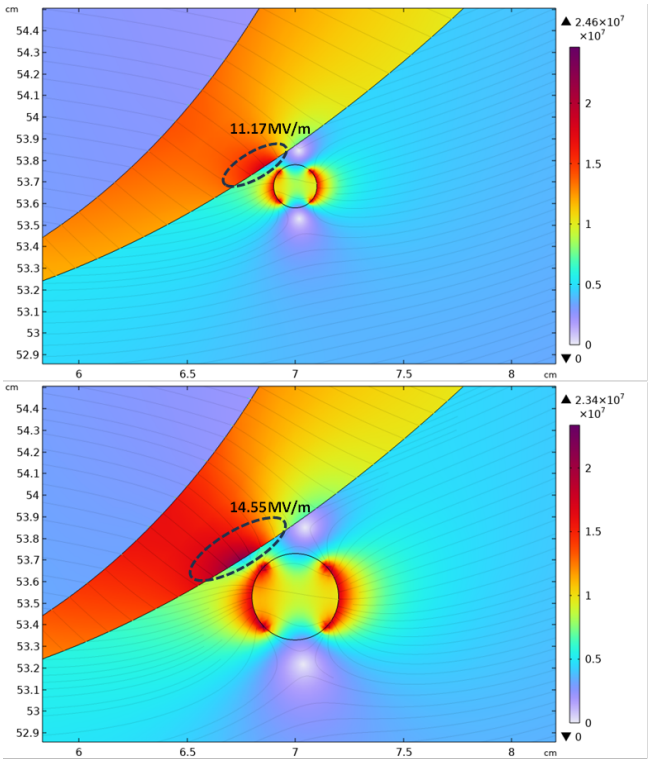

Fig. 15. Normal electric field on the inner surface for (a) r_v=1mm and d_{s1}=1mm, (b) r_v=2mm and d_{s1}=1mm.

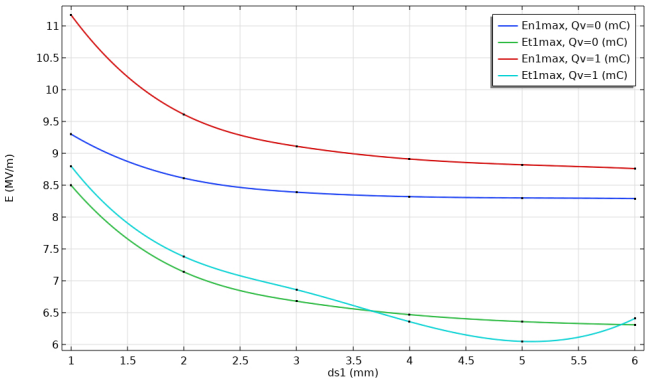

Fig. 16. Normal and tangential electric field for different spacing between void and the inner spacer surface.

high charge density because bigger field values are produced over a wider area of the spacer's surface when the void's radius is increased. Positive charges cause a drop in the field on the inner surface, whereas negative charges close to the central conductor contribute to an increase. The pattern here is the opposite of what occurs on the outer surface. In order to quantify these changes, the field enhancement factor, which is lower on the inner surface than it is on the outer surface, achieves maximum values of 1.45 for tangential fields and 1.38 for normal fields. The distribution of the electric field on the inner surface is more affected by a larger void than by a smaller void while the charge density remains constant. Both normal and tangential field distributions show this effect. With a charge density of 1000 μC/m2, the maximum field values on the inner surface can reach as high as 14.55 MV/m and 11.73 MV/m for normal and tangential fields, respectively. The link between the electric field and the separation between the void and the inner surface has been investigated, and it has been found that the field values fall more quickly when the separation is less than 3 mm.

Conflict of Interest

The authors have no conflict of relevant interest to this article can be used.

References

[1] B. Du, H. Liang, J. Li, and Z. Ran, "Electrical field distribution along SF_6/N_2 filled DC – GIS/GIL epoxy spacer," *IEEE Transactions on Dielectrics and Electrical Insulation*, vol. 25, no. 4, pp. 1202–1210, 2018.

[2] "Simulation study of electric influence caused by defects on uhv ac gis spacer, author=Wang, Haoran and Peng, Zongren and Guo, Zihao and Wang, Qingyu and Liao, Jintao and Zhang, Siyu, booktitle=2015 IEEE 11th International Conference on the Properties and Applications of Dielectric Materials (ICPADM), pages=676–679, year=2015, organization=IEEE,"

[3] F. Gutfleisch and L. Niemeyer, "Measurement and simulation of PD in epoxy voids," *IEEE transactions on Dielectrics and Electrical insulation*, vol. 2, no. 5, pp. 729–743, 1995.

[4] K. Wu, Y. Suzuoki, and L. Dissado, "The contribution of discharge area variation to partial discharge patterns in disc-voids," *Journal of Physics D: Applied Physics*, vol. 37, no. 13, p. 1815, 2004.

[5] G. C. Crichton, P. Karlsson, and A. Pedersen, "Partial discharges in ellipsoidal and spheroidal voids," *IEEE Transactions on Electrical Insulation*, vol. 24, no. 2, pp. 335–342, 1989.

[6] B. Ma, X. Wu, X. Li, X. Zhou, Q. Zhang, J. Li, and X. Han, "Study of the influence of void defect size on partial discharge characteristics in solid insulation," in *2018 IEEE International Conference on High Voltage Engineering and Application (ICHVE)*, pp. 1–4, IEEE, 2018.

[7] M. Hikita, M. Kozako, H. Takada, M. Higashiyama, T. Hirose, S. Nakamura, and T. Umemura, "Partial discharge phenomena in artificial cavity in epoxy cast resin insulation system," in *2010 IEEE International Symposium on Electrical Insulation*, pp. 1–5, IEEE, 2010.

[8] H. Illias, G. Chen, and P. L. Lewin, "Partial discharge behavior within a spherical cavity in a solid dielectric material as a function of frequency and amplitude of the applied voltage," *IEEE Transactions on Dielectrics and Electrical Insulation*, vol. 18, no. 2, pp. 432–443, 2011.

[9] H. Illias, G. Chen, and P. Lewin, "Measurement of partial discharge activities within two artificial spherical voids in an epoxy resin," in *2011 Annual Report Conference on Electrical Insulation and Dielectric Phenomena*, pp. 489–492, IEEE, 2011.

[10] H. V. P. Nguyen and B. T. Phung, "Void discharge behaviours as a function of cavity size and voltage waveform under very low-frequency excitation," *High Voltage*, vol. 3, no. 2, pp. 96–102, 2018.

[11] S. Morsalin, B. Phung, and A. Cavallini, "Measurement and modeling of partial discharge arising from different cavity geometries at very low frequency," *IEEE Transactions on Dielectrics and Electrical Insulation*, vol. 27, no. 4, pp. 1110–1118, 2020.

[12] T. Umemoto, S. Yoshida, Y. Otake, H. Muto, and M. Kurimoto, "Insulation lifetime characteristics of epoxy/tio 2 nanocomposite with internal void," in *2019 IEEE Conference on Electrical Insulation and Dielectric Phenomena (CEIDP)*, pp. 182–185, IEEE, 2019.

[13] D.-E. A. Mansour, K. Nishizawa, H. Kojima, N. Hayakawa, F. Endo, and H. Okubo, "Charge accumulation effects on time transition of partial discharge activity at GIS spacer defects," *IEEE Transactions on Dielectrics and Electrical Insulation*, vol. 17, no. 1, pp. 247–255, 2010.

[14] W. Haoran, P. Zongren, G. Zihao, W. Qingyu, L. He, and L. Lilan, "Electrical field influence of metallic particles and inner voids on UHV AC GIS spacer," in *2016 IEEE International Conference on Dielectrics (ICD)*, vol. 1, pp. 359–362, IEEE, 2016.

[15] H. Zhou, G. Ma, C. Wang, J. Wang, G. Zhang, Y. Tu, and C. Li, "Review of charge accumulation on spacers of gas insulated equipment at dc stress," *CSEE Journal of Power and Energy Systems*, vol. 6, no. 3, pp. 496–517, 2019.

[16] M. Ladani and P. Preetha, "Reduction of electric field stress on the surface contour and at the triple junction in UHVAC GIS by spacer design optimization," *International Journal of Emerging Electric Power Systems*, vol. 20, no. 2, p. 20180160, 2019.

[17] Y. Luo, J. Tang, Z. Pan, and C. Pan, "How temperature and pressure affect the electric field distribution in HVDC GIS/GIL: A numerical study," *IEEE Transactions on Dielectrics and Electrical Insulation*, vol. 28, no. 4, pp. 1334–1342, 2021.

[18] C. Li, C. Lin, B. Zhang, Q. Li, W. Liu, J. Hu, and J. He, "Understanding surface charge accumulation and surface flashover on spacers in compressed gas insulation," *IEEE Transactions on Dielectrics and Electrical Insulation*, vol. 25, no. 4, pp. 1152–1166, 2018.

[19] Z. Liang, C. Lin, F. Liang, W. Zhuang, Y. Xu, L. Tang, Y. Zeng, J. Hu, B. Zhang, C. Li, *et al.*, "Designing HVDC GIS/GIL spacer to suppress charge accumulation," *High Voltage*, vol. 7, no. 4, pp. 645–651, 2022.

[20] H. N. Afrouzi, A. Hassan, D. T. Y. Chee, K. Mehranzamir, Z. A. Malek, S. V. Mashak, and J. Ahmed, "In-depth exploration of partial discharge modelling methods within insulations," *Cleaner Engineering and Technology*, vol. 6, p. 100390, 2022.

[21] B. Du and H. Liang, *Epoxy-based Spacers for Gas Insulated Power Apparatus*. Springer, 2023.

[22] P. R. Manual, "Comsol multiphysics programming reference manual," 2021.

[23] H. Li, C. Wang, Z. Guo, H. Wang, S. Zhang, Z. Peng, and F. Ma, "Influences of semi-conductive coatings on the electric field distribution of GIS spacer interface," in *2015 IEEE 11th International Conference on the Properties and Applications of Dielectric Materials (ICPADM)*, pp. 887–890, IEEE, 2015.

[24] S. Chakravorti, *Electric field analysis*. Taylor & Francis Group, LLC, 2015.

[25] D. J. Griffiths, *Introduction to electrodynamics*. Cambridge University Press, 4th ed., 2017.

[26] S. Hore, S. Basak, N. Haque, S. Dalai, and M. Mukherjee, "Studies on the effect of void geometry and location on electric field distribution and partial discharge in xlpe insulated power cable by finite element analysis using comsol multiphysics simulation," in *2017 6th International Conference on Computer Applications In Electrical Engineering-Recent Advances (CERA)*, pp. 220–225, IEEE, 2017.

[27] Q. T. Algwari and D. N. Saleh, "Numerical modeling of partial discharge in a void cavity within high-voltage cable insulation," *IEEE Transactions on Plasma Science*, vol. 49, no. 5, pp. 1536–1542, 2021.

[28] B. Du, H. Liang, J. Li, and Z. Ran, "Electrical field distribution along SF_6/N_2 filled DC^- GIS/GIL epoxy spacer," *IEEE Transactions on Dielectrics and Electrical Insulation*, vol. 25, no. 4, pp. 1202–1210, 2018.